Supporting information:

X-ray diffraction (XRD) analysis of the sodium titanate nanofibers were carried out using a Rigaku Ultima IV multipurpose X-ray diffractometer equipped with Cu Ka radiation and fixed monochromator. An acceleration voltage of 40 kV and 20 mA current were applied. The XRD patterns were collected using a continuous scan mode and 2theta (2θ) angle from 5 to 60 degree with sampling width of 0.02 degree and scan speed of 1 degree/minute.

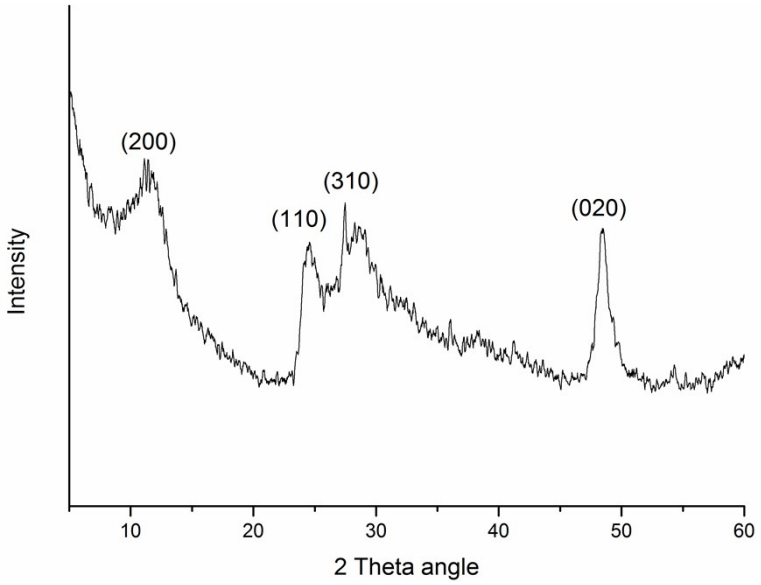

Figure S1: XRD pattern of sodium titanate nanofibers.

Figure S1 represents XRD pattern of sodium titanate nanofibers. The peaks at 2θ = 11.5º, 24.6º, 27.5º, and 48.5º correspond to the (200), (110), (310) and (020) planes of orthorhombic titanate phase. The structure of sodium titanate nanofibers therefore should be assigned to $Na_xH_{2-x}Ti_2O_5$.

SEM images were used to analyze the top surface pore size distribution and mean pore size for the asymmetric membranes. To this end, SEM images were treated and analyzed with

image treatment software Image-J as shown in Figure S2 (National Institutes of Health, Bethesda, Maryland, USA). For each membrane surface, 3 representative images were analyzed to get the statistical results.

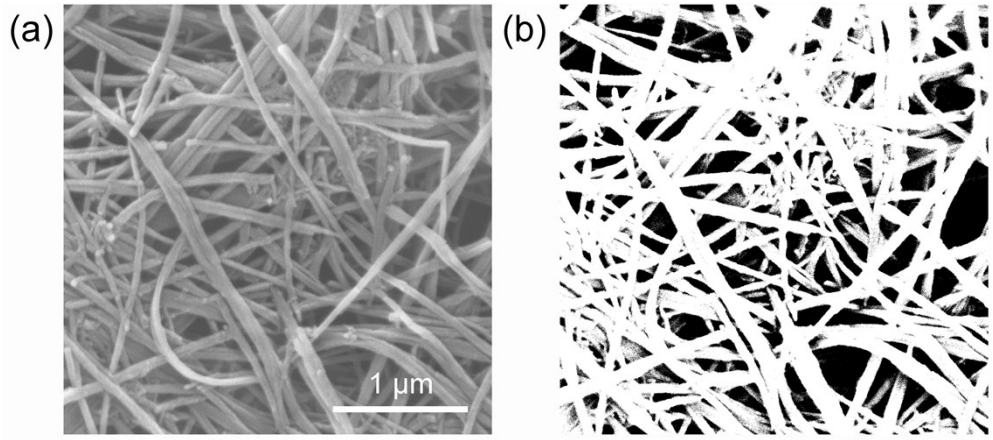

Figure S2: Top surface SEM images of asymmetric membrane based on sodium titanate nanofibers / cellulose microfibers prepared using 5 mL sodium titanate nanofibers stock solution, (a) initial image and (b) thresholded image treated by Image-J.

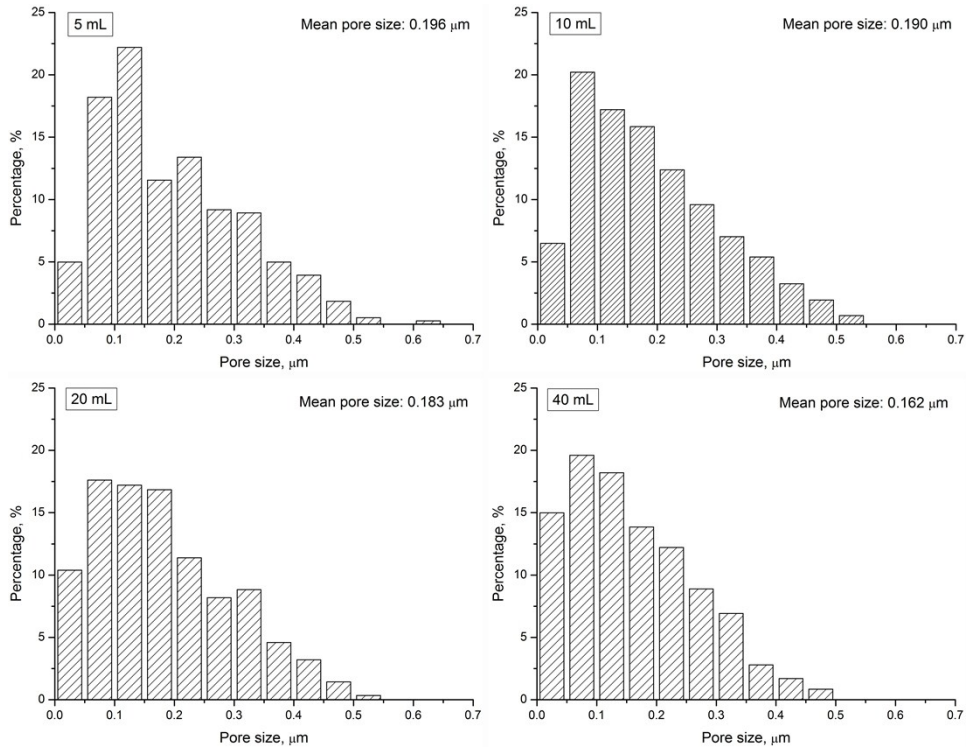

Figure S3: Top surface pore size distribution and mean pore size of the asymmetric membranes prepared using different volumes of sodium titanate nanofibers stock solution.

Figure S3 exhibits top surface pore size distribution and mean pore size of the asymmetric membranes obtained by means of the image treatment software Image-J. [1-5] *In this analysis, the asymmetric membranes were prepared using different volumes of sodium titanate nanofibers stock solution. The histograms in Figure S3 display narrow distribution of top surface pore size distribution for the asymmetric membranes. The top surface mean pore size of the asymmetric membranes decreased with increasing sodium titanate nanofiber stock solution volumes. More specifically, the top surface mean pore size of the asymmetric membranes decreased from 0.196 μm for the asymmetric membrane with 5 mL sodium titanate nanofibers to 0.162 μm for the asymmetric membrane with 40 mL sodium titanate nanofibers, representing a decrease of 17.3%. The narrow top surface pore size distribution for the asymmetric membranes*

is mainly due to the ultra-long sodium titanate nanofibers which formed compact and intertwined nanoporous structure of the selective layer. With increasing sodium titanate nanofiber stock solution volumes used for membrane preparation, the selective layers for the asymmetric membranes became more compacted, resulting in smaller top surface mean pore size.

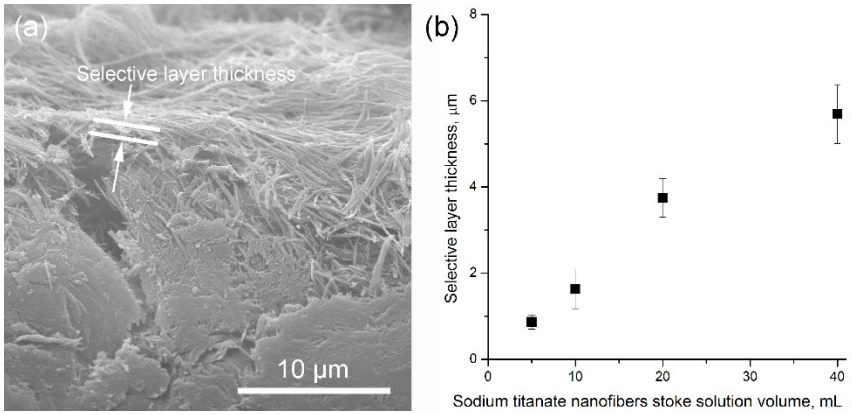

Figure S4: Selective layer thickness of the asymmetric membranes as function of sodium titanate nanofiber stock solution volume used for membrane preparation.

Selective layer thickness of the asymmetric membrane was measured using SEM cross-section images as shown in Figure S4 (a). The selective layer thicknesses for the asymmetric membrane prepared with 1 mL and 2.5 mL stock solution were not obtained because the microfiber substrate were not fully covered by these two volumes of sodium titanate nanofiber. In Figure S4 (b), It can be observed that the selective layer thickness of the asymmetric membranes increased with increasing sodium titanate nanofiber stock solution volume. More specifically, the thicknesses of the selective layer were 0.86 μm, 1.63 μm, 3.75 μm and 5.69 μm for the membranes prepared with 5 mL, 10 mL, 20 mL and 40 mL stock solutions, respectively.

The increase of selective layer thickness for the asymmetric membranes with increasing sodium titanate nanofiber stock solutions is attributed to the higher nanofiber content in larger volume of stock solution.

The mean droplet size and distribution of oil-in-water emulsion were measured using a visual process analyzer (Jorin-ViPA B HiFlo (Leicestershire, UK). Emulsion was analyzed immediately after preparation at room temperature.

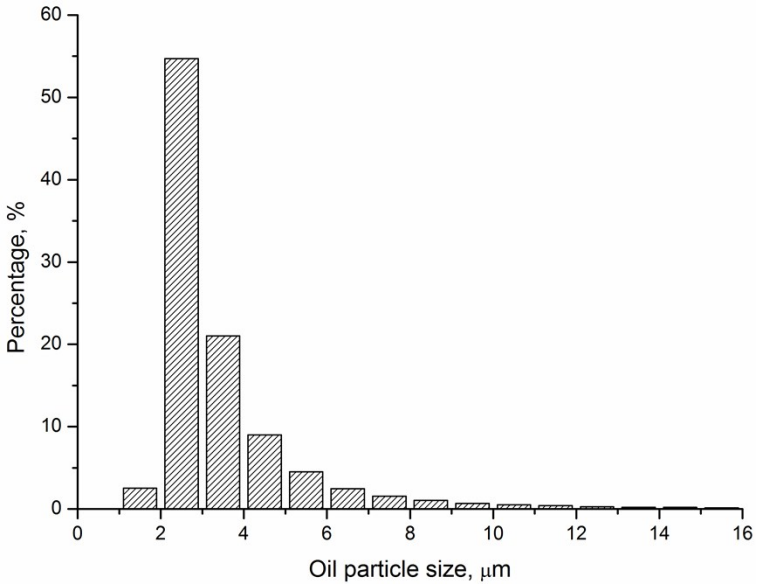

Figure S5: Sunflower oil droplet size distribution in as-prepared oil-in-water emulsions.

Figure S5 shows the oil particle size distribution for sunflower-oil-in-water emulsion. The resulting statistical plots display a narrow distribution of emulsion droplets mainly ranging from 1 to 8 μm in size. In addition, the sunflower-oil-in-water emulsion had a very small median droplet diameter of 2.86 μm. The narrow distribution of emulsion droplets and small median droplet diameter confirmed that the emulsion protocol used in this study was effective and controllable. Similar trends were observed for other prepared oil-in-water emulsions.

An optical microscopy Olympus IX73 (Shinjuku, Tokyo, Japan) was used to confirm the separation effect. This equipment was equipped with a digital camera coupled with an Olympus cellSens software allowing pictures to be recorded.

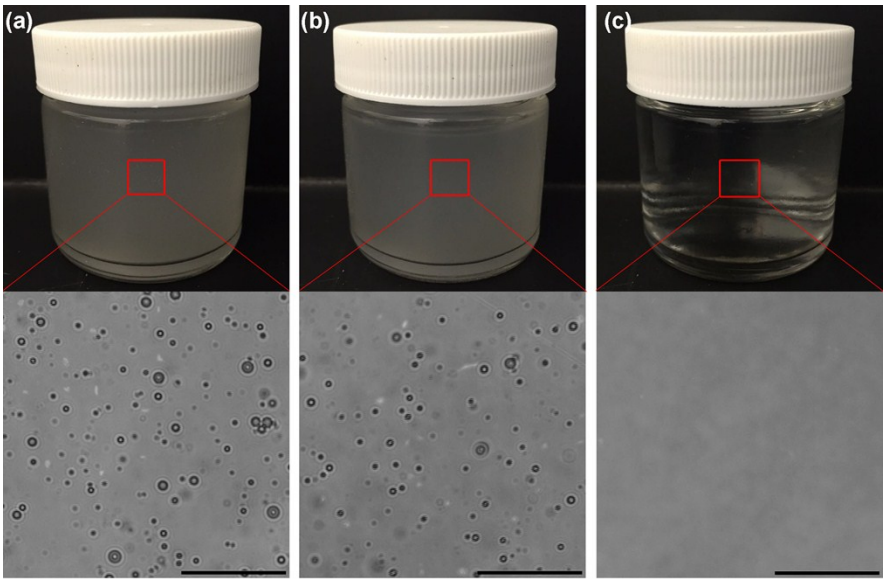

Figure S6: Photos and microscope images for (a) As-prepared sunflower oil-in-water emulsions (b) Filtrate of sunflower oil-in-water emulsions separated using cellulose membrane (c) Filtrate of sunflower oil-in-water emulsions separated using the asymmetric membrane with 5 mL sodium titanate nanofiber stock solution, the scale bar is 50 μm.

Digital photo of as-prepared milky sunflower oil-in-water emulsions is shown in Figure S6 (a). Dense oil droplets in micrometer-scale could be clearly observed in the corresponded optical microscope image. After separation using the cellulose filter under a transmembrane pressure of 5 kPa, no visible difference was found between the feed emulsions and the filtrate (see Figure S6 (b)), indicating a less separation efficiency due to the relatively loose porous structure of the cellulose membrane. However, after separation using the asymmetric membrane,

the collected filtrate had a significant change in color and light transmission as displayed in Figure S6 (c). No visible oil droplets were observed in the corresponded filtrate using optical microscope, indicating excellent separation efficiency.

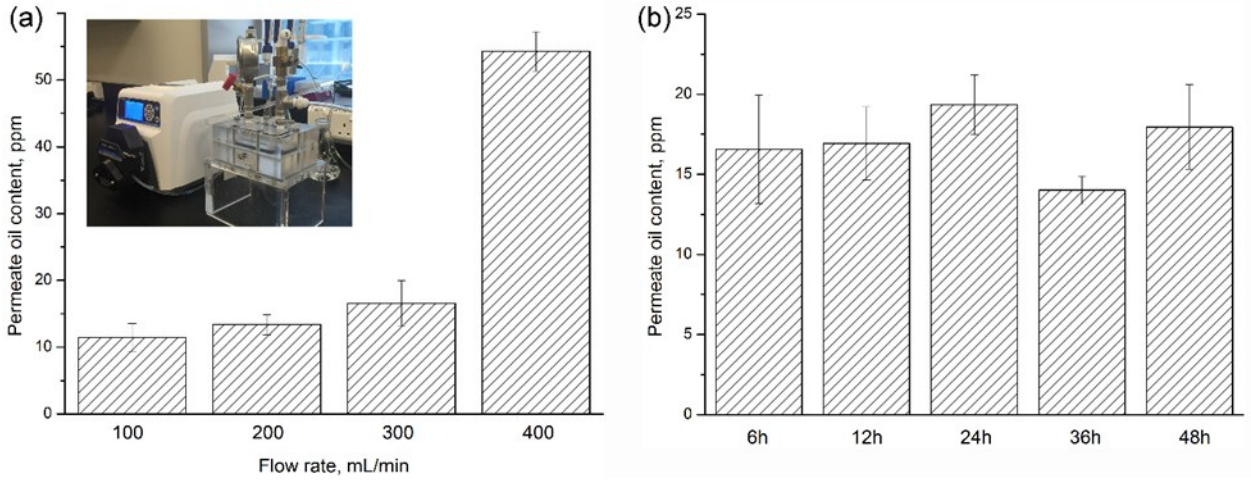

Figure S7: Oil content in the filtrates of sunflower oil-in-water emulsions filtrated by the asymmetric membrane after cross-flow filtration process with (a) different flow rates at a duration of 6 hours, (b) different filtration durations at a flow rate of 300 mL/min.

The stability of selective layer for the asymmetric membranes during cross-flow filtration process was investigated. As shown in Figure S7, the oil rejection property of asymmetric membrane can be stable with flow-rates lower than or equal to 300 mL/min under an investigation duration of 6 hours. More specifically, the sunflower-oil content in filtrate was below 20 ppm when the flow-rates were lower than or equal to 300 mL/min. With increasing flow-rate to 400 mL/min, the sunflower-oil content in filtrate increased to 54.3 ppm exceeding U.S discharge limit. The oil rejection property of the asymmetric membrane was then examined at different cross-flow filtration durations till to 48 hours at a fixed flow-rate of 300 mL/min. It was found that the rejection property of our asymmetric membrane was stable in our

investigated duration range, thanks to the combined effects of the ultra-long dimensions of sodium titanate nanofibers and PVA cross linking (as shown in Experimental part in main text). *The sunflower-oil content in filtrate was below 20 ppm after a cross-flow filtration process of 48 hours, indicating a good stability of our asymmetric membrane. We therefore recommend that the flow rate should be 300 mL/min and below under cross flow operation mode.*

Reference:

1. A. Akthakul, *Doctoral dissertation*, *Massachusetts Institute of Technology*, 2003.
2. S. Wu, F. Wildhaber, O. Vazquez-Mena, A. Bertsch, J. Brugger and P. Renaud, *Nanoscale*, 2012, **4**, 5718-5723.
3. R. Holdich, S. Kosvintsev, I. Cumming and S. Zhdanov, *Philos. Trans. A Math. Phys. Eng. Sci.*, 2006, 364, 161-174.
4. A. Morihama and J. Mierzwa, *Braz. J. Chem. Eng.*, 2014, **31**, 79-93.
5. E. Subtil, J. Mierzwa and I. Hespanhol, *Braz. J. Chem. Eng.*, 2014, **31**, 683-691.